Wind and Structures, *Vol. 33, No. 5 (2021) 367-381*
https://doi.org/10.12989/was.2021.33.5.367

CFD model validation with experimental tornado wind field & comparison of wind field in different tornado chambers

Sumit Verma and Rathinam P. Selvam*,

Department of Civil Engineering, University of Arkansas, Fayetteville, AR 72701, U.S.A.

(*Received March 3, 2021, Revised August 27, 2021, Accepted September 23, 2021*)

Abstract. Validation of CFD tornado wind field with experimental or field measurements is limited to comparison of tangential velocity profile at certain elevations above the ground level and few studies are based on comparison of pressure profile. However, important tornado vortex features such as touchdown swirl ratio (S_T), core radius (r_c), maximum tangential velocity (V_{tmax}), elevation of maximum tangential velocity (z_c) and pressure distribution over a range of varying swirl ratios which strongly influences tornado forces on a building have not been accounted for validation of tornado wind field. In this study, important tornado vortex features are identified and validated with experimental measurements; the important tornado features obtained from the CFD model are found to be in reasonable agreement with experimental measurements. Besides, tornado chambers with different geometrical features (such as different outlet size and location and total heights) are used in different works of literature; however, the effect of variation of those key geometrical features on tornado wind field is not very well understood yet. So, in this work, the size of outlet and total height are systematically varied to study the effect on important tornado vortex parameters. Results indicate that reducing outlet diameter in a tornado chamber increases S_T, Vtmax and z_c and decreases r_c. Similarly, increasing total height of tornado chamber decreases S_T, V_{tmax} and r_c whereas z_c remains nearly constant. Overall, it is found that variation of outlet diameter has a stronger effect on tornado wind field than the variation in total height of tornado chamber.

Keywords: 3D tornado simulation; CFD flow validation, Tornado chamber geometry variation

1. Introduction

A tornado is a non-synoptic severe weather phenomenon arising from cumulonimbus clouds. Historical records have shown that the direct economic loss due to tornadoes may amount to millions of dollars depending on the severity of tornado as inferred from Changnon (2009) and Simmons and Sutter (2011). Here, direct economic loss refers to the direct damage and loss of assets and properties. Indirect impacts add considerably to the economic losses. Similarly, deadly tornadoes have claimed the lives of hundreds of people over the years as emphasized in Molloy and Mihaltcheva (2013). Considering the financial losses and loss of human lives caused by tornadoes, it seems critical from a civil engineering standpoint to design and build structures resistant to tornadoes to minimize the financial losses and casualties. To be able to do so, it is necessary first to understand the detailed flow characteristics of tornado wind field. With the same motivation, experimental tornado chambers were built (e.g., Ward (1972), Church *et al*. (1977), Mishra *et al*. (2008), Mayer (2009), Sengupta *et al*. (2008), Haan *et al*. (2008), Haan *et al*. (2010), Hu *et al*. (2011), Hangan (2014)) and are now in operation. Despite being an important asset to study about the flow dynamics of tornado and loads induced by them on various structures, experimental tornado chambers have a drawback that their construction, operation, and maintenance is very costly. Besides, it is also challenging to acquire the near-surface velocities and pressure measurements in experimental tornado chambers (Tang *et al*. 2018a), which are important for evaluating tornado forces on buildings. In the recent times, Baker and Sterling (2019), using principles of similitude theory, have pointed out that experimental tornado simulation may not bear resemblance to real-world tornadoes as the experimentally simulated ones do not satisfy the requirement of kinematic and dynamic similarity. Several challenges with experimental tornado chambers have made computational studies a more attractive alternative. Besides, in the recent years, the cost constraint posed by experimental tornado chambers has been curbed to a great extent by Computational Fluid Dynamics (CFD) studies. In addition, the near-surface velocities and pressures can also be extracted with ease from CFD simulation results.

Most of the early CFD works were based on numerical modeling of tornado winds by an axisymmetric vortex (e.g., Harlow and Stein (1974), Rotunno (1977), Rotunno (1979)), the results from numerical model mostly entailed a qualitative comparison of tornado vortex features from CFD with experimental or real-world tornadoes (e.g., Rotunno (1979), Lewellen and Lewellen (1977, 2007), Nolan and Farrell (1999)). This was due to very limited experimental and field data available at that time. However, it is necessary to compare and validate CFD tornado flow field with experimental or field measurements to ensure that

*Corresponding author, Ph.D. Professor
E-mail: rps@uark.edu

ISSN: 1226-6116 (Print), 1598-6225 (Online)

CFD model follows the trend of real-world physical measurements. During a decade long period from 2004 to 2014, different experimental tornado chamber facilities were constructed to study about tornado vortices and loads induced by them on structures. As more experimental data became available, the trend to validate CFD models with experimental data became more prevalent.

In that regard, Ishihara *et al*. (2011) modeled a CFD tornado chamber based on dimensions of experimental tornado chamber used by Matsui and Tamura (2009). The CFD flow field was validated by comparing the tangential velocity profile from CFD with experimental measurements. However, the study was limited to two test cases of swirl ratio (i.e., S=0.31 and S=0.65) only and it is unclear whether tornado had touched down or not in either of the two swirl ratios. Liu and Ishihara (2015) developed a CFD model and validated it by comparing the time-averaged ground pressure profile from CFD with experimental measurements of Kikitsu *et al*. (2012). The pressure profile obtained from CFD model showed a good match with the experimental pressure profile, but the comparison was limited only to a single test case of swirl ratio, i.e., S=2.44. In addition, the information about tornado touchdown or the kind of flow structure represented by S = 2.44 is not readily available. Kuai *et al*. (2008), Yuan *et al*. (2016) and Yuan *et al*. (2019) modeled CFD tornado chamber based on ISU (Iowa State University) tornado chamber and computed the tornado wind field; however, a direct comparison of vortex features obtained from their CFD model with ISU experimental measurements was not presented. Gairola and Bitsuamlak (2019) modeled all the three major tornado chambers in the world (i.e., VorTECH, ISU tornado chamber and WindEEE dome) using Large Eddy Simulation (LES). However, validation of flow field was limited to ground pressure profile and tangential velocity profiles at certain specific elevations. Later, a simplified CFD model was proposed to represent the flow field of all the major experimental tornado chambers. Due to very high computational costs, majority of the work was done using the simplified CFD model based on RANS framework. The selection of RANS models instead of LES was a major limiting factor for the scope of the work. In the CFD community, it is well agreed that LES turbulence models are better and more accurate than RANS models as the mesh employed in LES simulation resolves the turbulent eddies in flow field rather than modeling the effect of eddies. For a complicated flow phenomena such as that of tornadoes, the selection of LES over RANS seems more appropriate for obtaining accurate CFD solutions. For a more recent review, Honerkamp *et al*. (2020) can be referred, which discusses the characteristics of tornado winds from meteorological, experimental, and computational standpoint.

From the review, it is found that validation of CFD tornado wind field is merely limited to comparison of tangential velocity profiles with experimental and field measurements and only few studies are based on comparison of pressure profiles. While the tangential velocity profile must compare well with experimental measurements for a good CFD model, but validation based on comparison of tangential velocity profile alone may not be a sufficient criterion for CFD flow validation since the tornado-induced forces on building depend on several other important features of tornado vortex such as the touchdown swirl ratio (S_T), maximum tangential velocity (V_{tmax}), core radii (r_c) and elevation of maximum tangential velocity (z_c). Similarly, as tornadoes are usually accompanied by a sharp drop in pressure at the center/core of tornado vortex which in turn strongly influences the induced pressures and forces on building, so, near-surface pressure distribution is also considered an important aspect for validating CFD tornado wind field.

1.1 Important tornado vortex parameters for CFD flow validation

In the following paragraphs, the important vortex parameters for validation of CFD flow field with experimental measurements are listed and the reasoning for identifying those parameters in CFD flow validation is discussed.

(i) Touchdown swirl ratio (S_T): Touchdown swirl ratio (S_T) is considered important because the severest suction pressure at centre of tornado vortex was observed at vortex touchdown in Tang *et al*. (2018a) and in the current work as well. Vortex touchdown marks an important phase in tornado-genesis since a fully developed downdraft flow exists at the core of tornado at this stage and it is beyond this critical phase the downdraft winds contact the ground surface and then starts translating in space causing mass destruction of settlement and structures falling in its path. Based on these arguments, touchdown swirl ratio (S_T) is considered an important engineering parameter for comparison and validation purpose.

(ii) Maximum tangential velocity (V_{tmax}): Tangential velocity of tornado is a major factor leading to severe damages in building envelope during tornadic events (Kashefizadeh *et al*., 2019), so, the magnitude of maximum tangential velocity (V_{tmax}) is considered another important parameter for validation of CFD tornado wind field.

(iii) Core radius (r_c): As per Alrasheedi and Selvam (2011), the impact produced on a structure due to tornado winds also depends on the ratio of core radius to plan area of building. For a given building, when the core radius is smaller compared to the size of building, the effect of tornadic winds is almost like SL winds with reduced force and pressure coefficients. Thus, a proper selection of core size seems important for Tornado Structure Interaction (TSI) study and accordingly, core radius (r_c) is identified as another important parameter for CFD flow validation.

(iv) Elevation of maximum tangential velocity (z_c): As stated above, the maximum tangential velocity is a major factor for building damage and it occurs at the location of core radius, so, it would be of interest from an engineering perspective to learn about the elevation of maximum tangential velocity (z_c) from the ground level as well as its location with respect to the height of buildings. Thus, the elevation of maximum tangential velocity (z_c) is also identified as an important parameter for CFD flow validation. Hence, the above four parameters (S_T, V_{tmax}, r_c and z_c) are considered for comparison with experimental measurements as well as for comparison of different tornado chambers.

Additionally, in any engineering design, the peak loads are of special significance. Because of the occurrence of largest suction pressures during touchdown (Tang at al. (2018 a, b)) and the dominance of high suction pressures on overall loading of structures as emphasized by Nasir and Bitsuamlak (2016), near surface pressure distribution with varying swirl ratios is also considered as an important aspect for CFD flow validation in this work. Also, the relevant datasets of pressure profiles are readily available from Tang *et al*. (2018b), so, the ground pressure profiles are also compared with TTU experimental measurements and is taken as an additional criterion for validation in section 3.1 below. However, validation of CFD flow field with respect to the important tornado features as emphasized above is lacking in the literature. In that regard, Verma and Selvam (2020) performed a preliminary analysis by comparing the near-surface pressure profiles obtained from their CFD model with TTU experimental data. The CFD pressure profiles showed good qualitative agreement with experimental data. However, the study was limited to qualitative comparison of near-surface pressure profiles and the aspect ratio (a) of tornado chamber was considered as unity. It is widely agreed upon that the aspect ratio of real-world tornadoes is less than unity as emphasized by Church *et al*. (1979) and unity usually represents the uppermost bound of aspect ratio making it a special case. The robustness of a particular CFD model is usually defined by its generality or its ability to reproduce, in general, any similar flow field that can be achieved in the experimental facility. Besides, a CFD model would be a closer reflection of real-world tornado if the obtained flow field from CFD were tested and validated with experimental data at lower values of aspect ratio. In the same spirit, the first part of this work attempts to compare and validate the CFD model with TTU experiment with respect to important tornado vortex parameters as discussed above at aspect ratio (a)=0.5 including a comparison of ground pressure distribution. This aligns well with the notion of tornadoes being a low aspect ratio (a < 1) phenomenon.

Similarly, the design of tornado chambers (i.e., geometrical features and flow generation mechanism) differs from one experimental facility to another whereas on the computational side, the computational domains differ with regards to geometry and boundary conditions. The effect of variation of geometrical features of tornado chamber on tornado wind field and on the important vortex parameters is still not understood very well. In that direction, Gillmeier (2019) and Gillmeier *et al*. (2019) studied the effect of geometric variation of tornado chamber on tornado wind field using surface pressure and velocity data and concluded that tornado wind field could still differ from one chamber to another even if the aspect ratio of chamber and swirl ratio of flow is kept similar. However, comparison of above identified four tornado vortex parameters was lacking in the study. Variation of these important features in different tornado chambers can change the flow field (or flow structure) of tornado as well as the interaction of tornado wind field with buildings thus resulting in different tornado forces and pressures on buildings. Different flow structures of tornadoes (single-celled, double-celled, and multi-vortex) have different wind velocity profile and pressure distribution; thus, they produce different loading conditions during their interaction with structures. Tornado pressures on buildings differs from one tornado chamber to another (C_p=-1 in TTU-VSII from Mishra *et al*. (2008) and C_p=-5 in ISU tornado chamber from Haan *et al*. (2010)). Similarly, different tornado chambers have different geometrical features such as different outlet sizes, total heights, etc. However, the effect of geometrical variations (such as the outlet diameter and height of tornado chamber) on tornado vortex parameters identified above is still not understood very well. So, in this work, the effect of variation of key geometrical features (size of outlet and total height) of tornado chamber is studied by systematically varying the outlet diameter and total height of tornado chamber and observing its effect on the important vortex parameters listed above.

1.2 Objectives of current work

As described in section 1.1 above, the current work is based on two major investigations, i.e. (1) validation of tornado wind with TTU experimental measurements at aspect ratio of 0.5 by comparing four tornado vortex parameters as described in section 1.1 above and (2) the effect of geometric variation (total height and outlet location and diameter of tornado chamber) on important vortex parameters. The objectives of current work are summarized below.

1. Validate CFD Tornado wind field with TTU (VorTECH) measurements at aspect ratio (a) of 0.5. The parameters considered for validation are as follows:

1.1 Comparison of S_T with TTU Experiment.

1.2 Comparison of core radius (r_c) at S=0.24 & S=0.78 with TTU Experiment as the representative cases of a single-celled and a double-celled vortex, respectively.

1.3 Comparison of maximum tangential velocity (V_{tmax}) as well as elevation of maximum tangential velocity (z_c) from CFD model with TTU Experiment.

1.4 Comparison of near-surface pressure field with TTU Experiment over a range of varying swirl ratios. ($0.15 \leq S \leq 0.96$)

2. Compare important vortex parameters from different tornado chambers and learn about the similarities and differences in flow structure of tornado vortices from different chambers.

2.1 Comparison of S_T, r_c, V_{tmax} and z_c by varying the outlet diameter of CFD tornado chamber.

2.2 Comparison of S_T, r_c, V_{tmax} and z_c by varying the total height of CFD tornado chamber.

2. Numerical setup

2.1 Computational modelling of VorTECH experimental facility

The cross-section of actual TTU tornado chamber along with its equivalent CFD model is shown in Fig. 1. The CFD chamber is modeled as a cylindrical column having inlet height of h_o, radius (r_{up}) and total height of $H=3r_{up}$. The

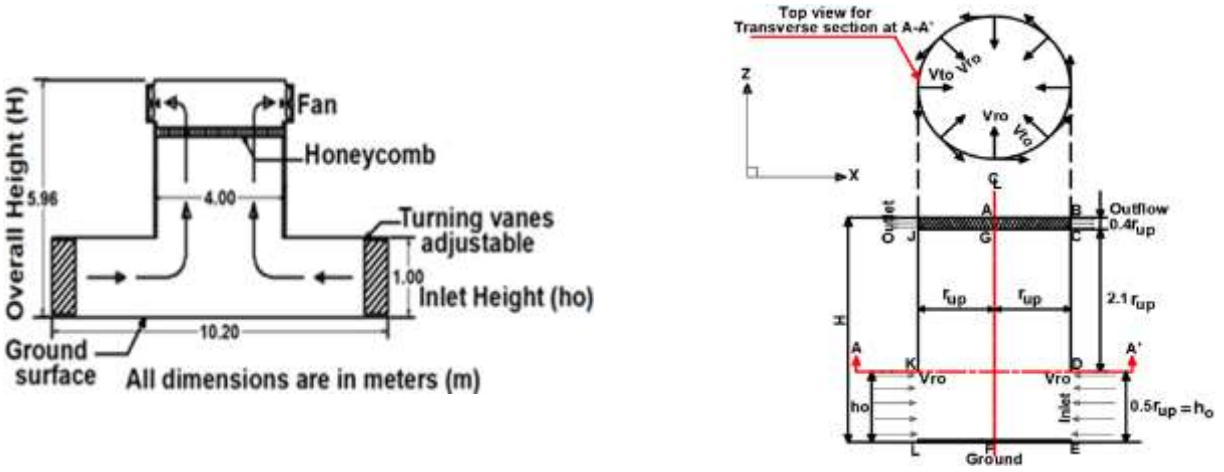

(a) (b)

Fig. 1 Cross-section of (a) VorTECH experimental facility (b) simplified CFD chamber at a=0.5

aspect ratio ($a=h_o/r_{up}$) of CFD tornado chamber is kept at 0.5. The fan outlet in experimental TTU chamber is replaced in the CFD model with an effective hole of height $0.4r_{up}$. More details on this issue are provided in Verma and Selvam (2020).

2.2 Governing equations and numerical schemes

The 3D incompressible Navier Stokes (NS) equation was used for flow computations. Large Eddy Simulation (LES) with Smagorinsky model was used for turbulence modelling. The smallest wavelength considered in LES modelling is around $4h_{min}$, where h_{min} is the smallest grid spacing. In the current case, the smallest wavelength is taken as $h_{min}=0.01h_o$, where h_o, is the inlet height (1 m).

The governing equations (continuity and momentum equation) for 3D incompressible flow used in the current work is expressed in tensorial notation as follows:

Continuity Equation:

$$\frac{\partial \bar{U}i}{\partial x_i} = 0 \tag{1}$$

Momentum Equation:

$$\frac{\partial \bar{U}i}{\partial t} + \frac{\partial \bar{U}i\bar{U}j}{\partial x_j} = -\frac{\partial \bar{P}}{\partial x_i} + 2\frac{\partial}{\partial x_j}\left(\nu + \nu_{sgs}\right)\bar{S}_{ij} \tag{2}$$

In Eq. (2), 'υ' is the kinematic viscosity of fluid whereas 'ν_{sgs}' is the turbulent kinematic viscosity, which is given by Eq. (3). In Eq. (3), C_{sgs} is the Smagorinsky constant taken as C_{sgs} = 0.1 and 'Δ' is the cube root of volume of a cell used in Smagorinsky model which is given by Eq. (4). Similarly, $\overline{S_{ij}}$ in Eq. (2) is the shear rate tensor, which is computed using Eq. (5) in the current work.

$$\nu_{sgs} = (C_{sgs}\,\Delta)^2\sqrt{2\,\overline{S_{ij}}\,\overline{S_{ij}}} \tag{3}$$

$$\Delta = \sqrt[3]{(\Delta x\ \Delta y\ \Delta z)} \tag{4}$$

$$\bar{S}_{ij} = \frac{1}{2}\left(\frac{\partial \bar{U}i}{\partial x_j} + \frac{\partial \bar{U}j}{\partial x_i}\right) \tag{5}$$

Staggered grid system using CVM (Control Volume Method) is used to discretize the computational domain for flow modelling. The diffusion terms of NS equation are approximated using CDS (Central Difference Scheme) while the convection terms are approximated using QUICK scheme. Line iteration method is used for solving the momentum equations. Continuity equation is satisfied using the SOLA procedure from Hirt and Cook (1972). Continuity and momentum equations are solved implicitly. Euler scheme (backward in time) is used while solving the equations and the Courant-Friedrichs-Lewy (CFL) condition is kept less than unity for stability of numerical scheme. The details of numerical schemes adopted for computation can be obtained from Selvam (1997).

Similarly, non-dimensional form of governing equations is used for the current work and the reference values considered for obtaining non-dimensional NS equation are (a) updraft radius (r_{up}) for length scale and (b) radial velocity at inlet height (V_{ro}) for velocity. Further details about the conversion of dimensional form of NS equations to non-dimensional form can be obtained from Cengel and Cimbala (2014). All the simulations were run for a total non-dimensional time of 25 units with a non-dimensional time step size of 'dt'=0.001 units. A cylinder of diameter '$2r_{up}$' and total height of '$3r_{up}$' makes up the computational domain for CFD model in the current work. A grid size of 75 × 75 × 70 with 393,750 nodes based on an orthogonal grid system is used for discretization of flow region. The current grid was tested for grid independence and further details about grid independence can be obtained from Verma and Selvam (2020).

2.2 Boundary conditions

A logarithmic velocity profile is used to model the inlet velocities in X and Y direction in the CFD tornado chamber. The axial profile of mean tangential and radial velocity from Tang *et al*. (2018a) shows logarithmic variation for radial and tangential velocity components, thus, a log profile for inlet velocity was chosen for the current work. The vertical velocity component is considered zero throughout the inlet height. The maximum non-dimensional

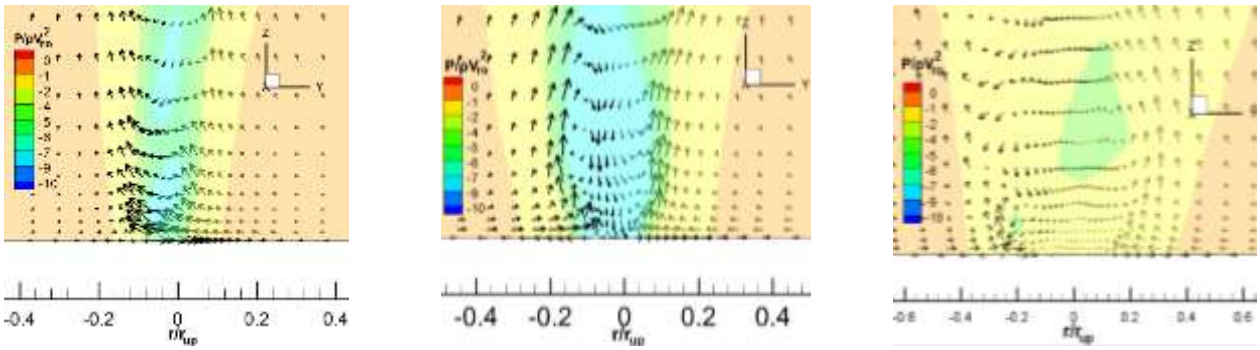

(a) (b) (c)

Fig. 2 Velocity vector diagram with pressure contour for the vortex obtained from CFD (a) before touchdown at S=0.22 (b) during touchdown at S=0.36 (c) after touchdown at S=0.50

radial velocity is taken as V_r ($z=0.5r_{up}$)=V_{ro}=1 and the corresponding tangential component is designated as V_{to}. The distribution of radial velocity from the base of tornado chamber (ground surface) up to the inlet height is expressed as a function of elevation (measured from the base of chamber) and is given as

$$V_r\ (z) = C_1\ \ln\left(\frac{z + z_o}{z_o}\right) = C_1\ \ln\left(1 + \frac{z}{z_o}\right) \quad (6)$$

The swirl ratio (S) for flow is calculated by

$$S = (V_{to}/V_{ro})/(2(h_o/r_{up})) \quad (7)$$

Using the defintion of 'S', the tangential component of velocity is obtained as

$$V_t\ (z) = 2\ V_r(z)\ S\ \left(\frac{h_o}{r_{up}}\right) \quad (8)$$

Regarding the outlet velocity boundary condition, a uniform normal velocity is provided at outlet and is equal to total inlet velocity. Other velocity components are calculated in the flow domain considering their normal derivatives to be zero. No-slip boundary condition is implemented at the top, bottom, and side walls. The roughness parameters used in the model are $z_o=0.00004r_{up}$ and $C_1=0.0924V_{ro}$. The Reynolds number considered for flow computation is 4×10^5, which is calculated at the inlet height (h_o) of tornado chamber.

3. Results

3.1 Validation of tornado wind field with TTU measurements

3.1.1 Comparison of touchdown swirl ratio (S_T) from CFD with TTU experiment

The computed flow field for S=0.22, 0.36 and 0.50 at aspect ratio (a)=0.5 are presented in Fig. 2. All these plots were taken at a plane passing through the center of computational domain and along the diametric axis of tornado chamber. In Fig. 2(a), it can be observed that the central downdraft has reached close to the ground surface for S=0.22 but without the occurrence of touchdown condition yet as indicated by the upward pointing velocity vectors near the base of CFD tornado chamber. This indicates that the aspect ratio of tornado chamber also influences the touchdown condition as with a similar tornado chamber configuration but with an aspect ratio of unity, touchdown condition was reported at S=0.22 in Verma and Selvam (2020). Similarly, from the flow visualizations in Fig. 2(b), it can be said that vortex touchdown occurs for S=0.36 as the velocity vectors can be observed to be touching the base of tornado chamber. Similarly, in Fig. 2(c), the swirl ratio case of S=0.50 represents a post-touchdown scenario with the formation of double-celled vortex. Tang *et al*. (2018b) also observed touchdown at S=0.36 for a=0.5. As the CFD model predicted touchdown swirl ratio very well for both a=0.5 and 1.0, it can be said that the CFD model can effectively predict the evolution of tornado wind field from experimental TTU tornado chamber facility.

3.1.2 Comparison of Vortex Core Radius with TTU Experiment

Core radius of tornado vortex is defined with reference to the location of maximum tangential velocity occurring in the flow domain. So, it is necessary first to determine the maximum tangential velocity before core radius can be estimated. However, due to vortex wandering phenomena as reported in studies such as Refan and Hangan (2018) and Gairola (2017), the centre of tornado vortex and the centre of tornado chamber may not coincide perfectly. Due to lack of a definite centre of tornado vortex, the tangential and the radial velocity cannot be computed from the x-component and y-component of velocity (i.e., 'U' and 'V' components respectively), which are obtained at the grid nodes after solving the NS equations. However, from observation of velocity vector visualization plots, it was inferred that a simplified approach as described in section 3.1.2.1 could be applied to obtain time-averaged core radius of tornado vortex, which is described next.

3.1.2.1 Procedure of determination of time-averaged core radius

From observation of velocity vector plots, it was inferred that velocity components close to the center of tornado chamber predominantly comprise of tangential

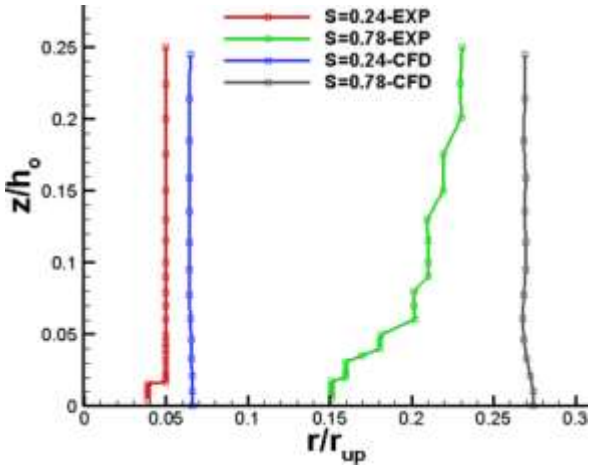

Fig. 3 Comparison of vertical profile of core radius from CFD with TTU experiment for S=0.24 & S=0.78

component whereas the radial component almost tends to 0. As tangential velocity is evaluated in XY-plane from the 'U' and 'V' velocity components, thus, the z-component of velocity (i.e., W-component) is not considered while determining time-averaged core radius. The procedure followed in this work to evaluate the core radius at each time step and subsequently the time-averaged core radius is described by the following steps:

(a) At a given time-step, the resultant velocity in horizontal plane is computed at different elevations (i.e., at each z-planes) as $U_{vze} = \sqrt{U^2 + V^2}$. At each z-plane, the maximum and the minimum U_{vze} is located and the distance between location of the maximum and the minimum U_{vze} gives the local core radius at each z-plane (i.e., at different elevations).

(b) While locating the minimum U_{vze}, the grid nodes lying within a region bounded by $0.4r_{up}$ on either side of the center of computational domain (in XY-plane) was considered. The distance $0.4r_{up}$ was selected based on the plots of experimental core radius versus elevation from Tang *et al*. (2018 a, 2018b).

(c) Among the different z-planes, the core radius obtained at a plane where the maximum U_{vze} (of all the U_{vze} occurring at different z-planes) is located and is called the representative core radius (r_c) for a given value of swirl ratio.

(d) The entire process consisting of steps from (a) to (c) is followed for every time-step once the flow attains statistically steady state. Here, the time-steps after non-dimensional time of 10 units is considered for time-averaging of core radius.

(e) Finally, the average of core radius values computed at different time-steps after the start of statistically steady state flow condition gives the time-averaged core radius for a given swirl ratio.

The vertical core profile reported in Tang *et al*. (2018b) for S=0.24 and S=0.78 from experiment (-EXP) was digitized as shown in Fig. 3 and the profiles for S=0.24 and S=0.78 (-CFD) were extracted from CFD simulation. For CFD core profiles, 15 grid nodes were selected from the base of simulator (reaching up to an elevation of $0.25r_{up}$). At each of the grid nodes, time-averaged core radius and elevation of core radius were computed using the procedure described in section 3.1.2.1.

The profile obtained from CFD simulation corresponding to S=0.24 showed an overall good similarity with experimental result of S=0.24 (both of which are representative of single-celled vortices in the respective simulation) with an average deviation (AD) of 0.016 times the updraft radius (r_{up}). The average deviation was calculated using Eq. (4), in which r_{EXP} represents the core radius from TTU experiment and r_{CFD} represents the core radius from CFD taken at a particular elevation (z=constant). Here, 'n' represents the total number of different elevation points considered

$$AD = \sum_{i=1}^{n} \frac{(r_{CFD} - r_{EXP})|_{z = const}}{n} \quad (9)$$

But for the double-celled vortex (corresponding to S=0.78), larger deviation as compared to S=0.24 is observed. The average deviation is about 0.066 times the updraft radius ($0.066r_{up}$). The observed discrepancy for S=0.78 may be attributed to flow measurement challenges in post-touched down tornado vortex in experimental tornado chamber as well as larger grid spacing in CFD tornado chamber. Due to greater turbulence in vortex core in post touchdown condition, it is suspected that taking flow measurements becomes greatly challenging at proper location as stated in Tang *et al*. (2018a). Also, the grid is coarser at regions far away from the center of CFD tornado chamber and thus may have led to the observed deviation. Besides comparing the vertical core profile, the values of core radii for both the swirl ratios was calculated and found to be $0.057r_{up}$ and $0.290r_{up}$ respectively. A more detailed comparison of the important tornado vortex parameters (S_T, V_{tmax}, r_c and z_c) is reported in Table 1 below.

3.1.3 Comparison of maximum tangential velocity and elevation of maximum tangential velocity from CFD model with TTU Experiment

As described briefly in section 1.1, the maximum tangential velocity is a significant contributing factor for building damage during tornadic events, thus, it is an important parameter of engineering significance. Similarly, the elevation of maximum tangential velocity (z_c) is also important from an engineering standpoint because it would be of interest for engineers/designers to know if the maximum tangential velocity is located at significant elevations from the ground level (higher than usual building heights) or not. If the occurrence of maximum tangential velocity were at an elevation much higher than usual building heights then, it would hint that the impact of maximum tangential velocity (resulting in positive aerodynamic pressures) would be somewhat reduced on buildings as the buildings would be then impacted by velocities of lesser magnitude. However, if the elevation of maximum tangential velocity were to occur at some place within the building height (of normal residential buildings), then, the elevation of occurrence of maximum tangential velocity as well as the magnitude of maximum tangential velocity would be of great engineering significance. So, in Table 1 below, the values of maximum tangential velocity

Table 1 Comparison of maximum tangential velocity and its elevation for aspect ratio (a)=0.5

S.N.	S	CFD			TTU		
		V_{tmax}/V_{ro}	r_c/r_{up}	z_c/r_{up}	V_{tmax}/V_{ro}	r_c/r_{up}	z_c/r_{up}
1	0.24	3.09	0.057	0.021	-	0.050	0.019
2	0.78	3.75	0.290	0.021	-	0.200	0.031

and the elevation of maximum tangential velocity are calculated from CFD for S=0.24 and S=0.78 and is reported below. For completeness, the values of core radius for S=0.24 and S=0.78 are also reported in Table 1.

In Table 1, the comparison of core radius (r_c) and elevation of maximum tangential velocity (z_c) shows good agreement between the CFD values and TTU measurements for S=0.24 whereas for S=0.78, there seems to be an overall agreement but with slightly higher deviation than that of S=0.24. A possible reason for larger deviation could be the turbulent vortex core beyond tornado touchdown for S=0.78. Beyond tornado touchdown, the vortex is in a highly turbulent and unsteady state, which creates several challenges in taking data measurements (Tang *et al*. 2018a), thus, some deviations may have occurred for S=0.78. For the CFD model, the maximum tangential velocity rises for S=0.78 as compared to S=0.24; however, the values could not be computed for TTU experimental datasets as the normalizing variable used in the current work is V_{ro} (radial velocity at inlet height of the tornado chamber, which is located at updraft radius, i.e., r_{up}=2 m) whereas the velocity measurement grid for TTU chamber extends only up to 70 cm from the center. Thus, a direct comparison for maximum tangential velocity could not be made and is not reported in Table 1.

From Table 1, it can be concluded that the core radius and the elevation of maximum tangential velocity shows reasonable agreement with TTU tornado chamber measurements and thus the CFD model demonstrates the potential to replicate tornado wind field of experimental TTU tornado chamber.

3.1.4 Comparison of near-surface pressure field with TTU experiment

The plot of radial distribution of ground pressure deficit relative to inlet obtained from the CFD model is presented in Fig. 4(a), which shows that there is a sharp drop in pressure at the core of vortex. For radial pressure profile in Fig. 4(a), the pressure at any radial location corresponds to the average of pressure values from two different time-steps towards the end of simulation time. These pressure values are taken along the diametric axis of tornado chamber. Further details about the time-averaging procedure adopted here can be obtained from Verma and Selvam (2020), similar procedure is followed in this work also.

As stated in section 3.1.2, due to vortex wandering, the pressure values can also change over time as the vortex moves in space but at this time, the spatial movement of vortex is not considered while evaluating the radial distribution of pressure. It was observed in Verma and Selvam (2020) that the pressure and tangential velocity at the center of computational domain varies in a periodic manner with respect to time and the magnitude of oscillation increases with increasing swirl ratios. Thus, for higher swirl ratios, it is recommended to consider a suitable length of time and obtain the flow properties averaged over that period for comparison. But time-averaging alone may not be sufficient as the vortex moves around in space over time as reported by several previous studies such as Refan and Hangan (2016), Gairola (2017) and Verma and Selvam (2020). Refan and Hangan (2016) used the technique of azimuthal averaging to rectify the error introduced in pressure distribution due to vortex wandering. However, in the current study, the major task was to compare and validate the flow field from TTU experiment and since the experimental results from Tang *et al*. (2018a, 2018b) does not account for this effect; so only time-averaging and not the effect of spatial wandering has been considered at this time in the current study.

It can be observed (in Fig. 4(a)) that the magnitude of drop in pressure goes on increasing with increasing swirl ratios up to S=0.36. As reported in section 3.1.1, this value corresponds to S_T for the present configuration of tornado chamber. After S=0.36, the magnitude of drop in pressure decreases momentarily for S=0.50 after which it starts to rise again for S=0.60 and S=0.96. At $S=S_T=0.36$, the critical transition of vortex takes place from a single-celled vortex to a double-celled vortex, which matches well with experimental observations of Tang *et al*. (2018b). A possible reason for the decrease in pressure drop for $S > S_T$ could be that the angular momentum and the flow energy of fluid mass gets distributed apparently with the formation of double-celled system and thus the sharp drop in pressure previously observed at the core center gets distributed within the two-celled vortex system. With increase in swirl ratio furthermore, the vortex again intensifies and, thus along with the double-celled system, the pressure goes on increasing again.

For comparison with TTU experiment (Tang *et al*. 2018b) in terms of dimensional pressure value, point X (indicated by an arrowhead) in Fig. 4(a) was considered. The point 'X' was considered because it is readily distinguishable compared to other points as the maximum drop in pressure is observed at that point. Similarly, the inlet height of tornado chamber is considered the location for reference pressure (at 0 Pa). The pressure deficit values are obtained with respect to the reference pressure. The value of non-dimensional pressure deficit observed at 'X' is -8.45. Using radial Reynolds number value of 3.11×10^5 from Tang *et al*. (2018b), the radial velocity at inlet (V_{ro}) was obtained as 2.43 m/s. Thus, the dimensional pressure value at 'X' was obtained by multiplying the non-dimensional pressure at 'X' with ρV_{ro}^2 where ρ=density of air (1.225 kg/m^3).

Thus, the value of dimensional pressure obtained at 'X' was -61.12 N/m^2 whereas the value of pressure obtained at

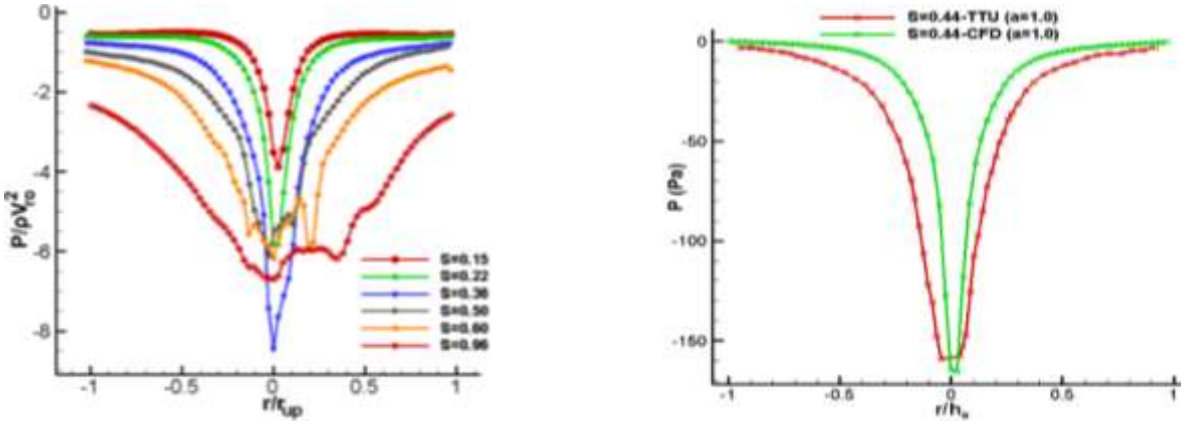

(a) (b)

Fig. 4 (a) Radial Pressure profile for different swirl ratios from CFD model at a=0.5 (b) Comparison of near-surface profile from CFD with TTU experiment for S=0.44 at a=1.0

the point corresponding to location 'X' from Tang *et al*. (2018b) was found to be -460 N/m^2. Although the CFD model was able to predict the nature of variation of radial pressure field reasonably well over the range of tested swirl ratios, it seems that the model does not capture the sharp pressure gradient well for S=0.36 and thus is unable to predict the peak pressure deficit.

However, when the model was run with swirl ratio of S=0.44 and at the aspect ratio (a)=1 as shown in Fig. 4(b), except for some discrepancy in capturing the pressure gradient close to vortex center, overall, the peak pressure deficit tallies well with experimental observations. The peak pressure deficit corresponding to CFD model is observed at -165.16 N/m^2 whereas that for TTU experiment is obtained at -158.17 N/m^2. Considering TTU measurement as the reference, the deviation in peak pressure deficit predicted by the CFD model is 4.42 %. Similarly, the normalized root mean squared error (NRMSE) for the overall pressure profile in Fig. 4(b) is about 15 %.

Hence, it can be concluded that the CFD model predicts variation of radial pressure distribution well over the range of swirl ratios for both the aspect ratios, i.e., a=1.0 and a=0.5 but the exact dimensional pressure values from CFD when compared with TTU experiment for a=0.5 shows some deviation in magnitude. The cause for such deviation is not very well understood at this time. On the other hand, the CFD model shows good agreement for S=0.44 at a=1.0 as shown in Fig. 4(b) and the pressure profiles over the range of swirl ratios as reported in Verma and Selvam (2020) exhibit an overall good agreement with experimental results. Further investigation is necessary to understand the cause of deviation in magnitude of dimensional pressure for the lower aspect ratio case.

Finally, the important tornado vortex parameters obtained from CFD model are compared with TTU experimental measurements for both aspect ratios (i.e., a=1.0 and a=0.5) in Table 2 below. In Table 2, it can be observed that the value of touchdown swirl ratio increases with the decrease in aspect ratio of tornado chamber. For the CFD model, the maximum tangential velocity decreases slightly whereas the core radius increases, and the elevation of maximum tangential velocity remains relatively constant with decrease in aspect ratio. Some deviation is observed in the comparison of core radius from CFD model with TTU experiment at aspect ratio of unity, which may be due to challenges in obtaining high resolution measurements in TTU tornado chamber. Similarly, the datasets presented in

Tang *et al*. (2018b) mostly pertains to that for two test cases of swirl ratio (i.e., S=0.24 and S=0.78), so, the comparison of maximum tangential velocity and core radius could not be made for S=0.36 at aspect ratio of 0.5 in Table 2. On the other hand, for aspect ratio of unity, the velocity measurements grid extends only up to within 0.7m from the center of tornado chamber in TTU tornado chamber whereas to obtain the ratio V_{tmax}/V_{ro}, the radial velocity at the updraft radius (at 2 m) would be required, which could not be obtained, so, the comparison is not made in Table 2.

From the collected results and the analyses done in section 3.1.1 to 3.1.4, it can be said that the CFD model shows good match with TTU experimental results in terms of touchdown swirl ratio and reasonable agreement in vertical core profile, values of core radius and elevation of maximum tangential velocity. So, the CFD model can replicate most of the important tornado vortex parameters from TTU tornado chamber facility. However, the comparison of ground pressure profile shows some deviation at aspect ratio of 0.5, the cause of which is not very well understood at this time. In this study, many important parameters of tornado vortex are considered for validation of CFD model and since most of the tornado vortex features compare reasonably well with TTU tornado chamber measurements, a validated CFD model is thus obtained for further studies.

Hence, in this section, validation of tornado wind field from CFD model is completed with TTU experimental measurements and in the following section 3.1.5, an analysis on the observed asymmetry of tornado wind field in a symmetrical computation domain is presented.

3.1.5 Analysis of asymmetry of tornado wind field from a symmetrical experimental and CFD tornado chamber

Although the tornado wind field is simulated in a symmetrical tornado chamber (both experimental facility and

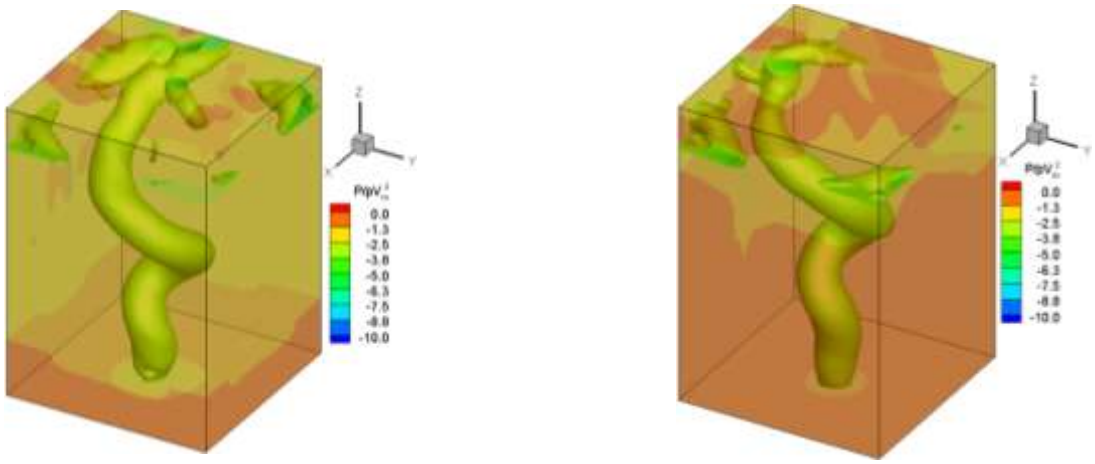

(a) (b)

Fig. 5 Nondimensional pressure iso-surface illustrating unsteady nature of the vortex at two different time instants for S= 0.36 (a) time=20 units (b) time=25 units

CFD), the obtained wind field is not exactly symmetrical because of highly unsteady nature of tornado vortex due to turbulent flow. In Fig. 5, the pressure iso-surface for swirl ratio case of S=0.36 at different time instants are plotted. At the time instant of t=20 units, the flow exits from negative X-direction whereas at the time instant of t=25 units, the flow seems to be exiting from negative Y-direction. Even after satisfying convergence criteria for governing equations and lowering residuals below the tolerance criteria, the flow inside a tornado chamber seems to be in a highly unsteady state, which may be a prominent cause for observed asymmetry in the flow field. As the flow occurs inside the tornado chamber at very high Reynolds number (Re ≈ 4×10^5), the flow is highly turbulent. Due to the turbulent eddies formed in flow field at high Reynolds number and the interaction of tornado vortex with turbulent eddies might be a probable factor for the observed asymmetry in the flow field.

Similarly, the pressure contour plots of tornado vortex are shown in Fig. 6 for swirl ratio (S)=0.36 at the ground level for different time instants. In Figs. 6(a)-6(d), a crosswire is drawn to demonstrate the center of tornado chamber and the blue colored suction spot in each of the figures represent the core of tornado vortex. It can be clearly noticed that the core of tornado vortex is in different places at different time instants. In other words, the core of tornado vortex moves around the center of tornado chamber over time. The spatial movement of core of tornado vortex over time is described in the literature by a term called "tornado vortex wandering", which is discussed in several studies in the literature such as Refan and Hangan (2018), Gairola (2017), Ashton *et al*. (2019) and the reference cited therein. Thus, the phenomenon of vortex wandering is also a significant factor contributing to the asymmetry of wind field in tornado chambers.

In section 3.1, validation of tornado wind field obtained from CFD model was completed with TTU experimental measurements and an analysis on observed asymmetry of wind field in symmetrical tornado chambers was presented. Now, in the following section, the effect of variation of geometrical features (outlet diameter and total height of tornado chamber) on tornado wind field is examined.

3.2 Comparison of important tornado vortex parameters (S_T, V_{tmax}, r_c and z_c) from different tornado chambers

Different tornado chambers in different parts of the world have differences in geometry and flow generation mechanism (Gairola and Bitsuamlak 2019). Tornado wind field and induced forces on buildings by tornado vortices have been studied in the past using experimental facilities of different geometry and flow generation mechanism and similarly on the CFD side, computational domain of different shapes with different boundary conditions have been used but how the inherent geometrical differences affect formation of tornado vortices is not understood very well. Furthermore, a good understanding about the effect of geometrical differences of tornado chambers on tornado vortex parameters (S_T, V_{tmax}, r_c and z_c) and consequently tornado-induced pressures on buildings is also lacking. To address the challenges arising from localized interpretation of flow field parameters in tornado chambers (with different geometry and flow generation mechanism), Gairola and Bitsuamlak (2019) proposed a generic CFD simulator whose dimensions were based on the flow parameters extracted from CFD simulation of the original tornado chamber facitlities. However, the two-step simulation procedure, particularly the CFD simulation by modeling the entire experimental facility in the first step is computationally very expensive and requires enormous computing power.

In this section, the four important tornado vortex parameters (S_T, V_{tmax}, r_c and z_c) identified in section 1.1 are compared from different tornado chambers by systematically varying the outlet diameter and the total height of tornado chamber. As the geometrical features and flow mechanism differs from one tornado chamber to another around the world, so, it would be a very tedious task to compare important tornado vortex parameters of each tornado chamber individually. To tackle with such

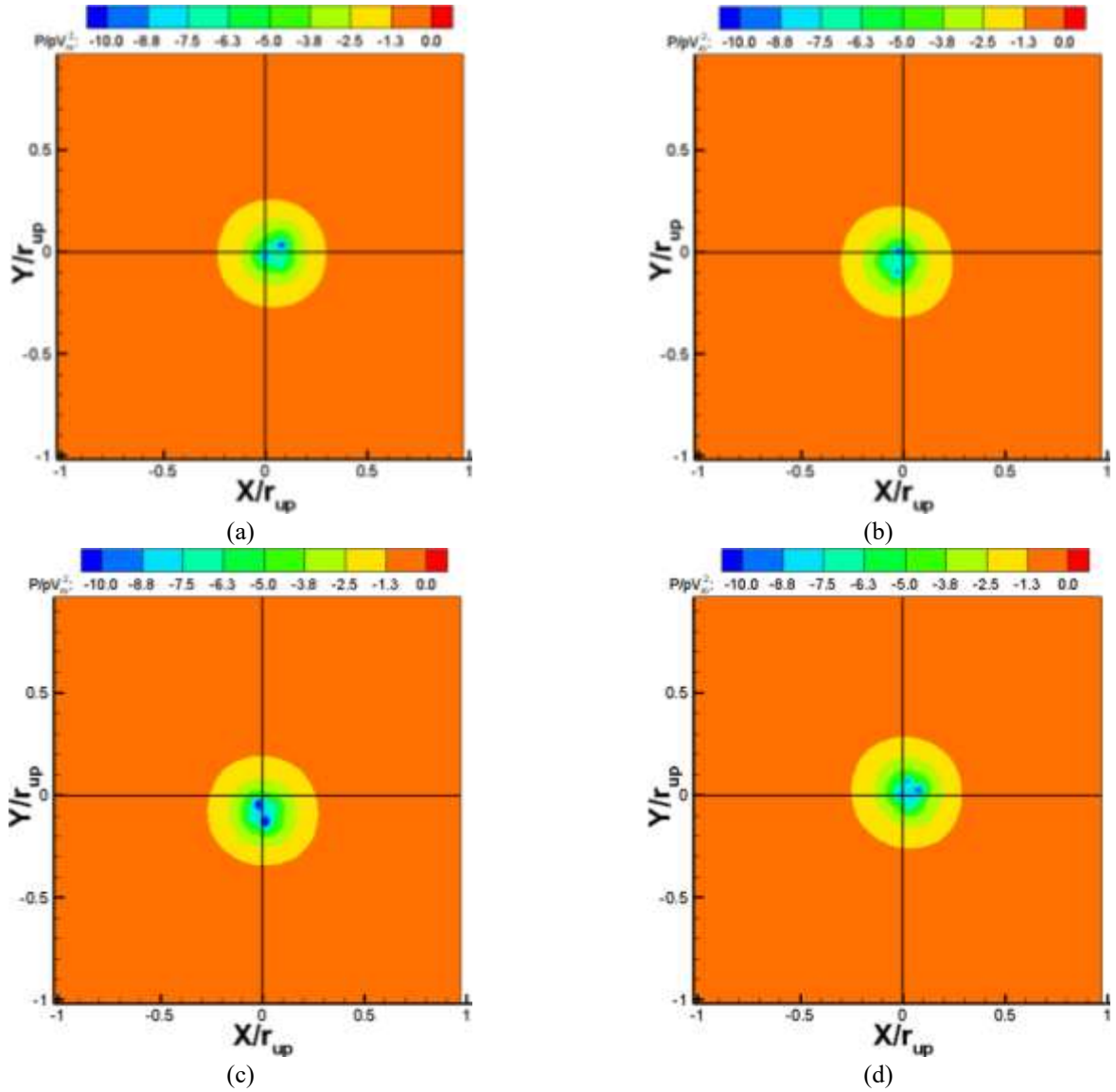

Fig. 6 Pressure contour plot taken at the ground plane of CFD tornado chamber for S=0.36 at different time instants to exhibit unsteady nature of tornado vortex (a) t=20.02 (b) t=21.69 (c) t=22.71 (d) t=25.09 units

challenge, the macroscale flow similarities such as the manner in which the air enters, progresses through and exits a tornado chamber were identified and the tornado chambers were categorized into 3 main categories viz. (a) Top Full Opening System (TFOS) (b) Top Partial Opening System (TPOS) (c) Side Opening System (SOS). As all the 3 categories of tornado chambers have cylindrical geometry and the two key dimensions for a cylindrical geometry are its diameter (or radius) and height, so, in the following sections, the diameter of outlet and the total height of tornado chamber are systematically varied to study its effect on tornado wind field.

The SOS type tornado chamber was already considered for TTU flow validation in section 3.1 and the important tornado vortex parameters for SOS type chambers for two aspect ratios (i.e., a=1 and a=0.5) were reported in Table 2. Now, in the following text, the effect of variation of outlet size on tornado vortex parameters (S_T, $V_{tmax,}$ r_c and z_c) is reported in section 3.2.1 while the effect of variation of total height of tornado chamber on vortex parameters is documented in section 3.2.2 below.

3.2.1 Comparison of S_T, $V_{tmax,}$ r_c and z_c from Different Tornado Chambers by Varying Outlet Diameter of Tornado Chambers

In this section, the influence of outflow rate (or the size of outlet) of tornado chamber on tornado wind field is examined. For that purpose, tornado vortex parameters (S_T, V_{tmax}, r_c and z_c) are compared for tornado vortices obtained by varying the outlet diameter of tornado chambers. The TFOS type vortex chamber as shown in Fig. 7(b) has a fully open outlet at the top. To study the effect of variation of outlet diameter on tornado wind field, the outlet diameter of TFOS chamber was gradually reduced so that the resulting chambers were transformed into the TPOS type chambers as shown in Fig. 7(c). As stated above, the outlet diameter (D_{out}) of tornado chamber was reduced from D_{up} (corresponding to the TFOS) to $0.75D_{up}$ and $0.50D_{up}$ (i.e., TPOS type) gradually.

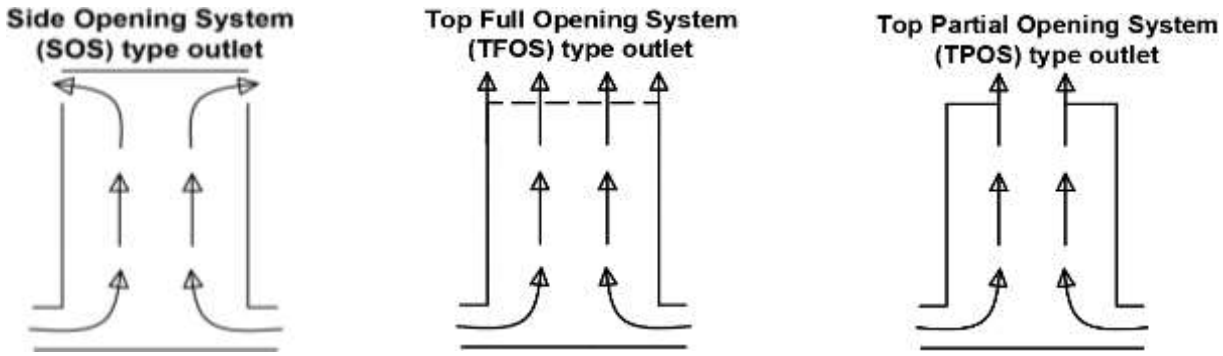

Fig. 7 Cross-section of tornado chambers (a) Side Opening System (SOS) (b) Top Full Opening System (TFOS) (c) Top Partial Opening System (TPOS)

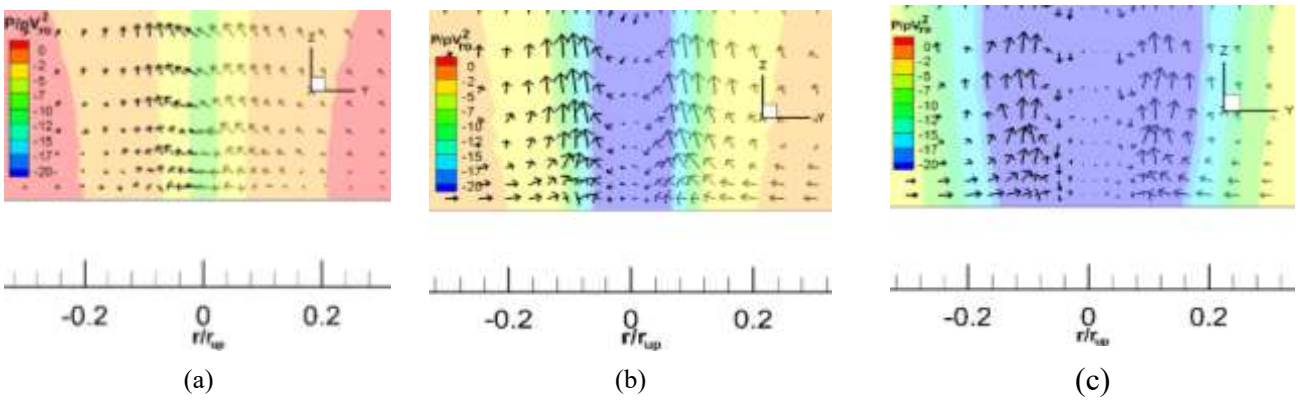

Fig. 8 Velocity vector diagram with pressure contour for the vortex obtained from CFD for TFOS chamber (a) before touchdown for S=0.15 (b) at touchdown for S=0.40 (c) after touchdown for S=0.80

1. S_T for TFOS type Chamber (D_{out} /D_{up}=1)

The computed flow fields from the TFOS type chamber (D_{out}=D_{up}) for S=0.15, 0.40 and 0.80 are shown in Fig. 8. In Fig. 8 (a), the computed flow field represents a single-celled vortex with all the velocity vectors rising upwards even in the core region (greenish color band) whereas in Fig. 8(b), vortex touchdown as indicated by the downward pointing arrows is observed for S=S_T=0.40. Similarly, in Fig. 8(c), a post-touchdown scenario is observed with a widened vortex core.

2. S_T for TPOS type Chamber (D_{out} /D_{up}=0.75)

As the outlet diameter of tornado chamber is reduced from D_{out}=D_{up} to D_{out}=0.75D_{up}, the value of touchdown swirl ratio is found to increase. The computed flow field for S = 0.15, 0.45 and 0.80 are shown in Fig. 9. The velocity vectors are pointing upward in the low pressure region (yellow color band) in Fig. 9(a) for S=0.15, whereas in Fig. 9(b) for S=0.45, downward pointing velocity vectors (cyan blue/violet color band) can be observed. Similarly, in Fig. 9 (c), post-touched down vortex with a widened vortex core is shown.

3. S_T for TPOS type Chamber (D_{out} /D_{up}=0.5)

By similar arguments presented above, vortex touchdown was confirmed for S=0.60 when the outlet diameter was further reduced to D_{out}=0.5D_{up}. The computed flow field for S=0.15, 0.60 and 0.80 are shown in Fig. 10.

From the parametric studies reported above, it can be concluded that the magnitude of S_T goes on increasing as the outlet diameter of tornado chamber is decreased gradually. Along with S_T, the pressure inside the tornado chamber is also found to be increasing as the outlet size is restricted gradually. A possible explanation for the observed outcome could be as follows: since, the flow is restricted by varying size of outlet while maintaining a constant inlet section, it results in an overall increase in pressure within the tornado chamber. It was observed previously in Verma and Selvam (2020) that the pressure inside vortex core are usually negative values, so, the increased pressure due to outlet size restriction probably tends to retard the process of vortex touchdown. Although negative pressures need not be necessary in the core and a steep gradient of pressure with a sharp drop at the center of tornado chamber facilitates the process of touchdown but increased pressure again due to restriction retards building up of such steep gradient in the core. Thus, restricting the size of outlet tends to raise the value of touchdown swirl ratio in a tornado chamber.

The values of touchdown swirl ratio, maximum tangential velocity, core radius and elevation of maximum tangential velocity for tornado chambers with different outlet conditions are reported in Table 3. Similarly, the important tornado vortex parameters from SOS type chambers at aspect ratio of unity and 0.5 (considered for

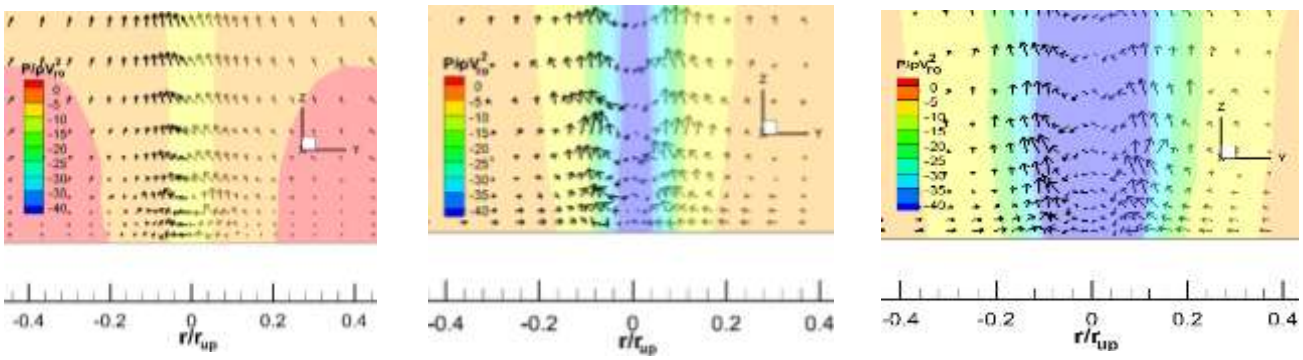

(a) (b) (c)

Fig. 9 Velocity vector diagram with pressure contour for the vortex obtained from CFD for TPOS chamber with D_{out}/D_{up}=0.75 (a) before touchdown for S=0.15 (b) at touchdown for S=0.45 (c) after touchdown for S=0.80

Table 3 Computed values of S_T, V_{tmax}, r_c & z_c for different outlet configuration

S.N.	Outlet condition	D_{out}/D_{up}	S_T	V_{tmax}/V_{ro}	r_c/r_{up}	z_c/r_{up}	% (ΔD_{out})	% (ΔS_T)
1	SOS (a = 1.0)	0.18	0.22	3.7	0.039	0.021	NA*	NA*
2	SOS (a = 0.5)	0.18	0.36	3.5	0.110	0.021	NA*	NA*
3	TFOS (D_{out} = 1.0D_{up})	1.00	0.40	4.9	0.073	0.034	-	-
4	TPOS (D_{out} = 0.75D_{up})	0.75	0.45	6.7	0.067	0.048	25	12.5
5	TPOS (D_{out} = 0.50D_{up})	0.50	0.60	9.6	0.063	0.078	50	50

*NA: Not applicable as the values come from a separate study

CFD flow validation in section 3.1) are also included in Table 3 to compare and analyze the effect of geometrical features of tornado chamber on tornado wind field. Besides, the percentage change in outlet diameter (% (ΔD_{out})) of tornado chamber and the percentage change in values of touchdown swirl ratio (% (ΔS_T)) for the TFOS and TPOS chambers are also reported in Table 3, in which the percentage change in outlet diameter and touchdown swirl ratio are evaluated by taking the outlet diameter of D_{out} = 1.0D_{up} and the corresponding touchdown swirl ratio (S_T) as reference values.

From Table 3, it can be observed that the value of touchdown swirl ratio (S_T) for SOS type chambers increases when the aspect ratio of tornado chamber is decreased, and the maximum tangential velocity also decreases slightly whereas the core radius of tornado vortex increases, and the elevation of maximum tangential velocity remains nearly constant. Furthermore, for the TFOS and TPOS type chambers, it can be observed that a subtle change in outlet diameter alone (while maintaining similar flow and geometry conditions) could result in different touchdown swirl ratios, different magnitude of maximum tangential velocity, core radius as well as different elevation of maximum tangential velocity. As the size of outlet diameter (for TFOS and TPOS chambers) goes on decreasing, the values of touchdown swirl ratio, maximum tangential velocity, and the elevation of occurrence of maximum tangential velocity goes on increasing whereas the core radius goes on decreasing. Core radius is defined at the location of maximum tangential velocity, which in turn is located at the highly sheared flow region formed due to interaction of updraft and downdraft flow velocities. As the size of outlet goes on decreasing, it is suspected that the size of such shear flow region also gets reduced, the effect of which is observed in reduced size of core radius. On the other hand, as the maximum tangential velocity differs significantly from one outlet configuration to another, it can be expected that similar effect would be propagated in tornado-induced pressures and forces during the interaction of tornado vortex with buildings in different tornado chambers. Hence, it can be said that the flow field obtained from tornado chambers with different geometry could also lead to different results and interpretation of tornado-induced pressures, forces, and moments on buildings in Tornado Structure Interaction (TSI) studies.

3.2.2 Comparison of S_T, V_{tmax}, r_c and z_c from different tornado chambers by varying total height of tornado chambers

Owing to simplicity of geometry of TFOS type chambers, it is considered in this section to study the effect of variation of total height of chambers on tornado vortex parameters (S_T, V_{tmax}, r_c and z_c). With a fully open outlet configuration at top, touchdown was found to occur at different swirl ratios when the total height of tornado chamber (H) was varied systematically. Touchdown swirl ratios for H=15h_o, 18h_o and 21h_o were found to be 0.45, 0.43 and 0.41 respectively as reported in Verma and Selvam (2021). This data is used for further analysis here.

From the obtained datasets, it can be said that **S_T** decreases with increasing height of tornado chamber. The dependence of S_T on total height (H), however, was found to be rather weak, which aligns with the idea of Gairola and Bitsuamlak (2019) that with a sufficiently tall tornado chamber of total height such as 15h_o, flow features become nearly independent of height. Further details about the modelling aspects and flow visualizations obtained from tall tornado chambers (i.e., H=15h_o, 18h_o and 21h_o) can be

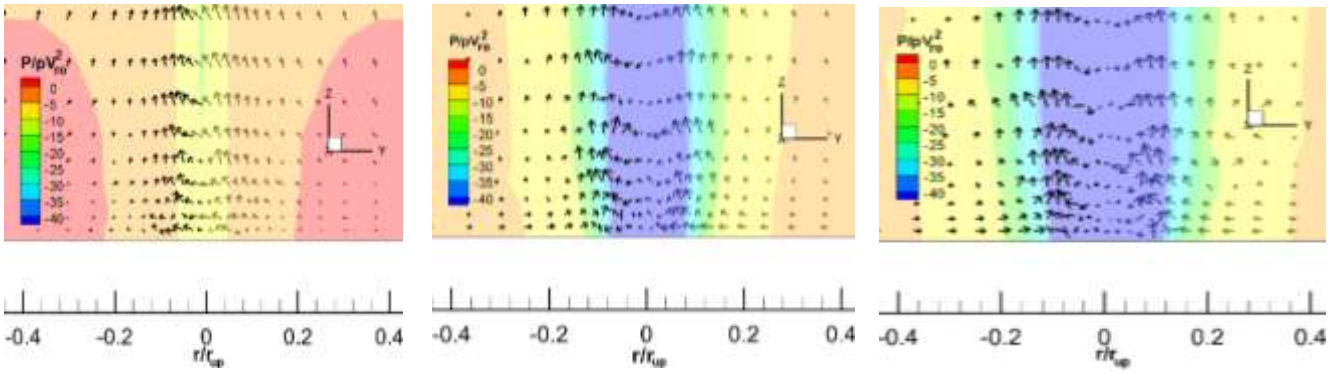

(a) (b) (c)

Fig. 10 Velocity vector diagram with pressure contour for the vortex obtained from CFD for TPOS chamber with D_{out}/D_{up}=0.50 (a) before touchdown for S=0.15 (b) at touchdown for S=0.60 (c) after touchdown for S=0.80

Table 4 Effect of Variation of Total Height of Tornado Chamber on S_T,V_{tmax}, r_c and z_c

S.N.	H	S_T	V_{tmax}/V_{ro}	r_c/r_{up}	z_c/r_{up}	% (ΔH)	% (ΔS_T)
1	$15h_o$	0.45	3.8	0.119	0.048	-	-
2	$18h_o$	0.43	3.7	0.113	0.052	20	4.44
3	$21h_o$	0.41	3.6	0.107	0.049	40	8.89

obtained from Verma and Selvam (2021).

In Table 4, the variation of important tornado vortex parameters (S_T, V_{tmax}, r_c and z_c) obtained from different total heights of the tornado chamber is reported. Besides, the percentage change in total height (% (ΔH)) of tornado chamber and the percentage change in touchdown swirl ratio (% (ΔS_T)) is also reported in Table 4, in which percentage change in total height and touchdown swirl ratio are evaluated by taking total height of $15h_o$ and the corresponding touchdown swirl ratio (S_T) as reference values. From the collected datasets in Table 4, it can be said that the value of touchdown swirl ratio decreases with increasing height of tornado chamber. Similarly, the maximum tangential velocity as well as the core radius of tornado vortex is also found to be decreasing with increase in total height of tornado chamber. However, neither an increasing nor a decreasing trend in elevation of maximum tangential velocity can be inferred from the collected datasets as the value of z_c first increases and then decreases with increase in total height of tornado chamber. On the other hand, it can be observed that increasing total height of tornado chamber by 20 % and 40 %, the values of touchdown swirl ratio decrease by 4.44% and 8.89% respectively.

From Tables 3-4, it can be concluded that the values of touchdown swirl ratio, maximum tangential velocity as well as elevation of maximum tangential velocity is significantly influenced due to variation of outlet diameter as compared to total height of tornado chamber. Furthermore, the magnitude of tangential velocity in Table 3 (i.e., tornado chambers with varying outlet diameter) is also higher compared to that in Table 4 (i.e., tornado chambers with varying total height). Similarly, increasing chamber height (% ΔH) by 40% causes a mere 8.89 % decrease in S_T (% ΔS_T) whereas decreasing outlet diameter (% ΔD_{out}) by 50 % causes S_T (% ΔS_T) to rise by 50%. From this observation, it can be said that variation of outlet diameter has a stronger effect on S_T than the variation of total height of tornado chamber. Overall, it can be concluded that changing the size of outlet has a stronger effect on the resulting tornado wind field than changing total height of tornado chamber.

4. Conclusions

A simple CFD model of tornado chamber developed in Verma and Selvam (2020) for LES based computations is used to obtain relevant tornado vortex features as obtained in experimental VorTECH facility in a reasonable timeframe and with reasonable accuracy. The major conclusions drawn from current work are summarized below.

- The important features of tornado vortex such as touchdown swirl ratio (S_T), core radius (r_c), maximum tangential velcoity (V_{tmax}), elevation of maximum tangential velocity (z_c) and pressure distribution that directly influences tornado forces on building are idenfied for CFD validation and the CFD model is validated with respect to important features of tornado vortex.
- While validating CFD tornado wind field with TTU experimental measurements, touchdown swirl ratio (S_T) matches well with experimental observation. Similarly, the values of core radius and elevation of maximum tangential velocity shows a reasonable agreement with experimental datasets. On the other hand, some deviations were observed in comparison of ground pressure profile for aspect ratio 0.5 of tornado chamber, the cause of which is not very well understood at this time. Whereas a good agreement was still obtained while comparing pressure profile at aspect ratio of unity. As a reasonable agreement was obtained in many important tornado vortex parameters, it is concluded that a validated CFD model is obtained for further studies.

• Tornado chambers are broadly classified into three major categories by identifying macroscale similarities in flow pattern, viz. (1) Side Opening System (SOS) tornado chamber (2) Top Full Opening System (TFOS) tornado chamber and (3) Top Partial Opening System (TPOS) tornado chamber, to compare similarities and/or differences in the resultant wind field obtained in tornado chambers with different geometrical features (i.e., different outlet diameters and heights of tornado chambers).
• Decreasing the size of outlet diameter increases the touchdown swirl ratio, the maximum tangential velocity, and the elevation of occurrence of maximum tangential velocity and decreases the core radius.
• Increasing total height of tornado chamber decreases the value of touchdown swirl ratio slightly. Similarly, the maximum tangential velocity as well as the core radius of tornado vortex are found to be decreasing with increase in total height of tornado chamber. However, any specific trend is not observed for the elevation of maximum tangential velocity as it increases first when height of tornado chamber is increased from $15h_o$ to $18h_o$ and then decreases when total height is increased further from $18h_o$ to $21h_o$.
• Overall, it is observed that decreasing the outlet diameter has greater influence on tornado wind field parameters than increasing the total height of chamber.

Acknowledgments

The research described in this paper was financially supported by the National Science Foundation under award number CMMI-1762999. The authors appreciate the unknown reviewers' input which helped to improve the paper extensively.

References

Alrasheedi, N.H and Selvam, R.P. (2011), "Tornado forces on different building sizes using computer modeling", *2011 ECTC Proceedings*, *ASME Early Career Technical Conference*, Hosted by ASME District E and University of Arkansas, Fayetteville.

Ashton, R., Refan, M., Iungo, G.V. and Hangan, H. (2019), "Wandering corrections from PIV measurements of tornado-like vortices", *J. Wind Eng. Ind. Aerod.*, **189**, 163-172. https://doi.org/10.1016/j.jweia.2019.02.010.

Baker, C. and Sterling, M. (2019), "Are tornado vortex generators fit for purpose?" *J. Wind Eng. Ind. Aerod.*, **190**, 287-292. https://doi.org/10.1016/j.jweia.2019.05.011.

Cengel, Y.A. and Cimbala J.M. (2014), *Fluid Mechanics: Fundamentals and Applications*, McGraw Hill, New York, NY, U.S.A.

Changnon, S.A. (2009), "Tornado losses in the United States", *Nat. Haz. Rev.*, **10**(4), 145-150. https://doi.org/10.1061/(asce)1527-6988(2009)10:4(145)

Church, C.R., Snow, J.T., Baker, G.L. and Agee E.M. (1979), "Characteristics of tornado-like vortices as a function of swirl ratio: a laboratory investigation", *J. Atmos. Sci.*, **36**(9), 1755-1776.https://doi.org/10.1175/1520-0469(1979)036<1755:COTLVA>2.0.CO;2

Church, C.R., Snow, J.T. and Agee, E.M. (1977), "Tornado vortex simulation at Purdue University", *Bull. Amer. Meteor. Soc.*, **58**(9), 900-909. https://doi.org/10.1175/1520-0477(1977)058<0900:TVSAPU>2.0.CO;2

Gairola, A. (2017), *Generic Numerical Tornado Model for Common Interpretation of Existing Experimental Simulators*, Master's thesis, University of Western Ontario, London, Ontario, Canada.

Gairola, A. and Bitsuamlak, G. (2019), "Numerical tornado modeling for common interpretation of experimental simulators", *J. Wind Eng. Ind. Aerod.*, **186**, 32-48. https://doi.org/10.1016/j.jweia.2018.12.013.

Gillmeier, S. (2019), An Investigation Concerning the Simulation of Tornado-Like Vortices", Ph.D. Dissertation, University of Birmingham, Birmingham, U.K.

Gillmeier, S., Sterling, M. and Hemida, H. (2019), "Simulating tornado-like flows: The effect of the simulator's geometry", *Meccanica*, **54**, 2385-2398. https://doi.org/10.1007/s11012-019-01082-4

Haan Jr. F.L, Balaramudu, V.K. and Sarkar, P.P. (2010), "Tornado-induced wind loads on a low-rise building", *J. Struct. Eng.*, **136**(1), 106-116. https://doi.org/10.1061/(ASCE)ST.1943-541X.0000093.

Haan, F.L., Sarkar, P.P. and Gallus, W.A. (2008), "Design, construction and performance of a large tornado simulator for wind engineering applications", *Eng. Struct.*, **30**(4), 1146-1159. https://doi.org/10.1016/j.engstruct.2007.07.010.

Hangan, H. (2014), "The wind engineering energy and environment (WindEEE) dome at Western University, Canada", *Wind Engineers, JAWE*, **39**(4), 350-351. https://doi.org/10.5359/jawe.39.350.

Harlow, F.H. and Stein L.R. (1974), "Structural analysis of tornado-like vortices", *J. Atmos. Sci.*, **31**(8), 2081-2098. https://doi.org/10.1175/1520-0469(1974)031<2081:SAOTLV>2.0.CO;2

Hirt, C.W. and Cook, J.L. (1972), "The calculation of three-dimensional flows around structures and over rough terrain", *J. Comput. Phys.*, **10**(2), 324-340. https://doi.org/10.1016/0021-9991(72)90070-8.

Honerkamp, R., Yan, G. and Synder, J.C. (2020), "A review of the characteristics of tornadic wind fields through observations and simulations", *J. Wind Eng. Ind. Aerod.*, **202**, 104195. https://doi.org/10.1016/j.jweia.2020.104195.

Hu, H., Yang, Z., Sarkar, P. and Haan, F. (2011), "Characterization of the wind loads and flow fields around a gable-roof building model in tornado-like winds", *Exp Fluids*, **51**, 835. https://doi.org/10.1007/s00348-011-1102-6.

Ishihara, T., Oh, S. and Tokuyama Y. (2011), "Numerical study on flow fields of tornado-like vortices using the LES turbulence model", *J. Wind Eng. Ind. Aerod.*, **99**(4), 239-248. https://doi.org/10.1016/j.jweia.2011.01.014.

Kashefizadeh, M.H, Verma, S. and Selvam, R.P. (2019), "Computer modelling of close-to-ground tornado wind-fields for different tornado widths", *J. Wind Eng. Ind. Aerod.*, **191**, 32-40. https://doi.org/10.1016/j.jweia.2019.05.008.

Kikitsu H., Okuda Y., Kawai H. and Kanda J. (2012), "Experimental study on characteristics of tornado-induced wind force on a low-rise building", *Proceedings of the 22nd National Symposium on Wind Engineering*, 209-214. https://doi.org/10.14887/kazekosymp.22.0.209.0.

Kuai, L., Haan, F.L.J., Gallus, W.A.J. and Sarkar, P.P. (2008), "CFD simulations of the flow field of a laboratory-simulated tornado for parameter sensitivity studies and comparison with field measurements", *Wind Struct.*, **11**(2), 75-96. https://doi.org/10.12989/WAS.2008.11.2.075.

Lewellen, D.C. and Lewellen, W.S. (2007), "Near-surface intensification of tornado vortices", *J. Atmos. Sci.*, **64**(7), 2176-2194. https://doi.org/10.1175/JAS3965.1.

Lewellen, W.S. and Lewellen, D.C., Sykes, R.I. (1997), "Large-eddy simulation of a tornado's interaction with the surface", *J. Atmos. Sci.*, **54**(5), 581-605. https://doi.org/10.1175/1520-0469(1997)054<0581:LESOAT>2.0.CO;2.

Liu, Z. and Ishihara, T. (2015), "A study of tornado induced mean aerodynamic forces on a gable-roofed building by the large eddy simulations", *J. Wind Eng. Ind. Aerod.*, **146**, 39-50. https://doi.org/10.1016/j.jweia.2015.08.002.

Matsui, M. and Tamura, Y. (2009), "Influence of swirl ratio and incident flow conditions on generation of tornado-like vortex", *Proceedings of EACWE 5*, Florence, Italy, July 19th-23rd. https://doi.org/10.1400/116522.

Mayer, L.J. (2009), *Development of a Large-Scale Simulator*, Master Thesis, Texas Tech University, Lubbock, U.S.A.

Mishra, A.R., James, D.L. and Letchford, C.W. (2008), "Physical simulation of a single-celled tornado-like vortex, Part B: wind loading on a cubical model", *J. Wind Eng. Ind. Aerod.*, **96**(8-9), 1258-1273. https://doi.org/10.1016/j.jweia.2008.02.027.

Molloy, S.L. and Mihaltcheva, S. (2013), "1.01 - Extreme weather events". Editor(s): Roger A. Pielke, *Climate Vulnerability*, Academic Press, 3-16. https://doi.org/10.1016/B978-0-12-384703-4.00103-9.

Nasir, Z. and Bitsuamlak, G.T. (2016), "Computational modeling of tornadic load on a tall building", *CSCE Annual Conference*, London Convention Center, London, Ontario, Canada, June.

Nolan, D.S. and Farrell, B.F. (1999), "The structure and dynamics of tornado-like vortices", *J. Atmos. Sci.*, **56**(16), 2908-2936. https://doi.org/10.1175/1520-0469(1999)056<2908:TSADOT>2.0.CO;2.

Refan, M. and Hangan, H. (2016), "Characterization of tornado-like flow fields in a new model scale wind testing chamber", *J. Wind Eng. Ind. Aerod.*, **151**, 107-121. https://doi.org/10.1016/j.jweia.2016.02.002.

Refan, M. and Hangan, H. (2018), "Near surface experimental exploration of tornado vortices", *J. Wind Eng. Ind. Aerod.*, **175**, 120-135. https://doi.org/10.1016/j.jweia.2018.01.042.

Rotunno, R. (1977), "Numerical simulation of a laboratory vortex", *J. Atmos. Sci.*, **34**(12), 1942-1956. https://doi.org/10.1175/1520-0469(1977)034<1942:NSOALV>2.0.CO;2.

Rotunno, R. (1979), "A study in tornado-like vortex dynamics", *J. Atmos. Sci.*, **36**(1), 140-155. https://doi.org/10.1175/1520-0469(1979)036<0140:ASITLV>2.0.CO;2.

Selvam, R.P. (1997), "Finite element modelling of flow around a circular cylinder using LES", *J. Wind Eng. Ind. Aerod.*, **67-68**, 129-139. https://doi.org/10.1016/S0167-6105(97)00068-8.

Sengupta, A., Haan, F.L., Sarkar, P.P. and Balaramudu, V. (2008), "Transient loads on buildings in microburst and tornado winds", *J. Wind Eng. Ind. Aerod.*, **96**(10-11), 2173-2187. https://doi.org/10.1016/j.jweia.2008.02.050.

Simmons, K.M. and Sutter D. (2011), *Economic and Societal Impacts of Tornado*, American Meteorological Society, Boston, U.S.A. https://doi.org/10.1007/978-1-935704-02-7.

Tang, Z., Feng, C., Wu, L., Zuo, D. and James, D.L. (2018a), "Characteristics of tornado-like vortices simulated in a large scale ward type simulator", *Bound. Lay. Meteorol.*, **166**, 327-350. https://doi.org/10.1007/s10546-017-0305-7.

Tang, Z., Zuo, D., James, D., Eguchi, Y. and Hattori, Y. (2018b), "Effects of aspect ratio on laboratory simulation of tornado-like vortices", *Wind Struct.*, **27**(2), 111-121. http://dx.doi.org/10.12989/was.2018.27.2.111.

Verma, S. and Selvam, R.P. (2020), "CFD to VorTECH pressure field comparison & roughness effect on flow", *J. Struct. Eng.*, **146**(9), 04020187-1. https://doi.org/10.1061/(ASCE)ST.1943-541X.0002766.

Verma, S. and Selvam, R.P. (2021), "Effect of height of the tornado chamber on vortex touchdown", In: Rushi Kumar B., Sivaraj R., Prakash J. (eds) *Advances in Fluid Dynamics. Lecture Notes in Mechanical Engineering*. Springer, Singapore. https://doi.org/10.1007/978-981-15-4308-1_38.

Ward, N.B. (1972), "The exploration of certain features of tornado dynamics using a laboratory model", *J Atmos. Sci.*, **29**(6), 1194-1204. https://doi.org/10.1175/1520-0469(1972)029<1194:TEOCFO>2.0.CO;2.

Yuan, F., Yan, G., Honerkamp, R, Kakkattukuzhy, M.I, Zhao, M. and Mao, X. (2019), "Numerical simulation of laboratory tornado simulator that can produce translating tornado-like wind flow", *J. Wind Eng. Ind. Aerod.*, **190**, 200-217. https://doi.org/10.1016/j.jweia.2019.05.001.

Yuan, F., Yan, G., Honerkamp, R., H., Isaac, K.M. and Ruoqiang, F. (2016), "Effects of chamber shape on simulation of tornado-like flow in a laboratory", *Wind engineering for natural hazards-modeling, simulation, and mitigation of windstorm impact on critical infrastructure*, Reston. https://doi.org/10.1061/9780784415153.ch08.

TK